

Heritable small RNAs regulate nematode benzimidazole resistance

Mostafa Zamanian^{1,2}, Daniel E. Cook^{1,3}, Daehan Lee⁴, Junho Lee⁴, and Erik C. Andersen^{1,5,6*}

¹Department of Molecular Biosciences, Northwestern University, Evanston, IL, USA

²Department of Pathobiological Sciences, University of Wisconsin-Madison, Madison, WI, USA

³Interdisciplinary Biological Science Program, Northwestern University, Evanston, IL, USA

⁴Institute of Molecular Biology and Genetics, Department of Biological Sciences, Seoul National University, Seoul, Korea

⁵Robert H. Lurie Comprehensive Cancer Center, Northwestern University, Chicago, IL USA

⁶Northwestern Institute on Complex Systems, Northwestern University, Evanston, IL USA

*erik.andersen@northwestern.edu

Parasitic nematodes impose a debilitating health and economic burden across much of the world¹. Nematode resistance to anthelmintic drugs threatens parasite control efforts in both human^{2,3} and veterinary⁴ medicine. Despite this threat, the genetic landscape of potential resistance mechanisms to these critical drugs remains largely unexplored. Here, we exploit natural variation in the model nematode *Caenorhabditis elegans* to discover quantitative trait loci (QTL) that control benzimidazole sensitivity and show that piwi-interacting RNAs (piRNAs) are capable of regulating benzimidazole resistance. We narrowed a major-effect albendazole QTL to a small piRNA-enriched region of the *C. elegans* genome and demonstrate that the albendazole-resistance phenotype results from strain-specific piRNA variation that is dependent on the function of the piRNA-associated argonaute *prg-1*. We identified candidate piRNAs causal to the resistance phenotype and putative genes targeted for silencing by downstream 22G RNAs. We further show that piRNAs may regulate benzimidazole susceptibility in the related model nematode *C. briggsae*. Our results indicate that small RNAs require consideration in drug resistance mechanisms in nematodes, because the piRNA pathway and related small RNA pathways are conserved in many medically and agriculturally important parasitic nematodes. This finding has significant implications for parasite control and the management of drug resistance in other phyla and systems.

The sustainability of chemotherapy-based parasite control is jeopardized by our deficient knowledge of potential mechanisms of anthelmintic resistance and a paucity of molecular markers to detect and to slow the spread of resistance alleles in parasite populations^{4–8}. Traditional approaches to identify anthelmintic resistance markers rely on surveying candidate genes for polymorphisms⁹. Known mechanisms of nematode benzimidazole resistance have been limited to alterations of the drug target beta-tubulin^{9–12}. However, polymorphisms in beta-tubulin genes do not explain all interspecific and intraspecific variation observed in benzimidazole efficacy¹³ or in responses to different benzimidazole derivatives^{14,15}. A more complete understanding of potential pathways to parasite benzimidazole resistance is necessary to help discover loci that are predictive of drug response. Although *C. elegans* has been historically indispensable to the discovery of mechanisms of action for benzimidazoles and other anthelmintics¹⁶, genetic variation within *C. elegans* has only recently been exploited to study phenotypic variation in anthelmintic responses¹⁷.

We examined natural variation in *C. elegans* responses to three widely used benzimidazoles (albendazole, fenbendazole, and thiabendazole). Dose responses were performed on a set of genetically diverged strains using a high-throughput pipeline¹⁸ (see Methods and Supplementary Methods) to quantify the effects of anthelmintics on animal fitness traits (size, feeding behavior, and fecundity) relevant to anthelmintic mechanisms of action in parasitic nematodes^{19,20}. Drug concentrations that exhibited high broad-sense heritability (Supplementary Fig. 1) were chosen for quantitative genetic mappings. To assess the potential effects of drug dose on the genetic architecture of drug sensitivity, two concentrations of fenbendazole and thiabendazole were selected. We identified quantitative trait loci (QTL) that control for observed differences in benzimidazole susceptibility using a linkage mapping approach. Benzimidazole-response phenotypes were measured for a collection of 292 *C. elegans* recombinant inbred advanced intercross lines (RIALs) created from a cross of the laboratory strain N2 and a Hawaiian strain CB4856¹⁸. Correlation of these control (no drug)-regressed phenotypic data with strain genotype data led to the discovery of 14 QTL that each explain greater than 5% of trait variation for the tested drugs (Figure 1A, Supplementary Table 1), with many of these QTL spanning multiple animal fitness traits (Supplementary Fig. 2). The primary trait groupings are confirmed by the correlation

structure of measured parameters and robust across summary statistics for distributions of these parameters (Supplementary Fig. 3). Benzimidazole sensitivity involved the contribution of multiple loci for many drug-trait combinations. Within this complex trait landscape, we identified QTL that are common but also some that are unique across drugs and doses.

We discovered a major QTL associated with the effects of albendazole on animal size traits. This QTL is localized to a 441 kb interval on chromosome IV (15.47 - 15.91 Mb) and explains 36% of albendazole-induced variation in animal length between the parental strains (Figure 1B). Recombinant strains with the N2 genotype at this locus are more resistant to incubation in 12.5 μ M albendazole than those strains with the CB4856 genotype, with CB4856 animals exhibiting a significantly greater decrease in length (Figure 1C). This major-effect albendazole QTL extends to pharyngeal pumping and is also associated with small differences in brood size (Supplementary Fig. 2). An overlapping QTL associated with animal size and pumping behavior was identified for 30 μ M fenbendazole as well. Subsequent analyses are presented for the albendazole QTL using the length trait with the highest significance score. The difference in albendazole response between the parental strains is approximately 45% of the difference between CB4856 and a *ben-1* mutant in the N2 background (Supplementary Fig. 4). Mutations in the parasite homologs of *ben-1* are known to result in clinically significant benzimidazole resistance, and this comparison underscores the potential importance of the amount of resistance explained by the major albendazole QTL on chromosome IV.

The QTL interval contains 17 protein-coding genes with coding variants and falls within the large piwi-interacting RNA (piRNA) cluster on chromosome IV (13.5 - 17.2 Mbs)²¹. To narrow this interval to a smaller region, we phenotyped near-isogenic lines (NILs) with QTL regions from either the N2 or CB4856 strains introgressed into the opposite genetic background (Figure 2A). NILs with the N2 genotype spanning the 15.57 - 15.65 Mb interval of chromosome IV exhibited resistance to albendazole and, conversely, NILs with the CB4856 genotype in this region were albendazole-sensitive (Figure 2B). We expect that the variant(s) of largest effect fall in this narrowed interval. Significant differences among NILs within the resistance and sensitive groupings suggested that additional variants and epistatic interactions within the complete QTL interval could influence albendazole susceptibility. In light of this complexity, we considered both the complete QTL interval and the NIL-narrowed interval in subsequent analyses.

The NIL-narrowed interval was annotated with known variants distinguishing N2 and CB4856 and their estimated functional consequences (Figure 2C, Supplementary Tables 2 and 3). We considered protein-coding and non-coding RNA (ncRNA) variation as potentially causal to the albendazole-resistance phenotype. Only three proteins in the narrowed interval are predicted to have altered functions as a result of single nucleotide variants (SNVs). However, the plausibility of these candidate genes was dampened by a number of factors. *Y105C5A.508* is curated as a short and likely pseudogenic transcript, which shares no homology with proteins in species with available sequence data. Additionally, we did not detect expression of this gene using RNA-seq in either the N2 or CB4856 strains. The gene *pqn-79* has a predicted coding variant (Thr194Ala) but belongs to a highly redundant protein family that has > 99.5% sequence identity with at least three other homologs. None of these homologs exhibits coding variation, but the possibility of a dominant-negative or gene dosage effect cannot be ruled out. The gene *Y105C5A.8* codes for a protein of unknown function that is predicted to contain a splice-donor variant, but we found no differences in splice form abundance between N2 and CB4856 for this gene. We hypothesized that albendazole resistance is more likely a function of variation in the non-coding RNA (ncRNA) complement, specifically the piRNA-encoding genes. No variation was observed for other ncRNA biotypes.

To test the hypothesis that variation in piRNAs underlies benzimidazole resistance, we first examined the overall effect of the broader primary *C. elegans* piRNA cluster on variation in albendazole response. Reciprocal N2 and CB4856 NILs were generated via introgression of the 13.37 - 17.23 Mb region of chromosome IV from each strain into the opposite genetic background. NIL strains that contained the N2 piRNA cluster in an otherwise CB4856 genetic background were equally as resistant to albendazole as the N2 parent strain, and the CB4856 piRNA cluster completely conferred the CB4856-sensitivity phenotype to the resistant N2 strain (Figure 3A). Next, we analyzed the responses of small RNA pathway mutants to albendazole in an effort to perturb the large number of diverse piRNAs. 21U-RNAs/piRNAs are regulated by the Piwi Argonaute PRG-1²². Therefore, we hypothesized that albendazole sensitivity should be dependent on *prg-1* function. We tested mutants in all three Argonaute genes that encode proteins that interact with primary small RNAs immediately upstream of WAGO-associated 22G RNA generation (*ergo-1*, *alg-4*; *alg-3*, and *prg-1*)²³. ERGO-1 and ALG-3/4 engage 26G RNAs, while PRG-1 coordinates the processing of piRNAs. Among mutations in these genes, only loss of *prg-1* conferred albendazole sensitivity in the resistant N2 background (Figure 3B). These data indicate that the albendazole-sensitivity phenotype is specific to the piRNA pathway, and that genetic variation in piRNA function, through loss or gain of specific piRNAs or through variants in shared piRNAs, is a mechanism of benzimidazole resistance in nematodes. Furthermore, the direction of the *prg-1* effect in the N2 genetic background suggests that the CB4856 strain harbors a loss or reduction of piRNA function causing albendazole sensitivity.

We employed a dual RNA and small RNA-seq approach to more comprehensively annotate variants within the primary *C. elegans* piRNA cluster, focusing on the major-effect albendazole QTL contained within it. These data allowed us to more precisely resolve differences in the piRNA complements of N2 and CB4856 (Supplementary Table 4) and to narrow the candidate list of albendazole-resistance determinants to specific genes and the piRNAs that potentially target them. Our pipeline combines piRNA, 22G RNA, and mRNA expression and variation data (see Methods and Supplementary Methods) to prioritize candidate genes that fit the expected profile of anti-correlated mRNA expression and antisense 22G RNA expression. This approach resulted in 283 genes that exhibit differential expression of both mRNA and 22G RNA between strains. Among these, 68 genes display higher levels of gene-specific CB4856 mRNA expression coupled to higher levels of gene-specific N2 22G RNA expression (Figure 3C). The candidate list includes genes associated with drug metabolism and transport (e.g., *cyp-29A2* and *cyp-33A1*), cuticular collagens (e.g., *col-71*), enzymes of interest (*ugt-37*), and large numbers of genes enriched in the germline or that are regulated by various xenobiotic stimuli. Homology-based searches were used to identify prioritized genes that contained predicted binding sites for putative piRNAs unique to either strain (Supplementary Table 5).

To compare benzimidazole-resistance loci across nematode species, we examined variation in the responses of *Caenorhabditis briggsae* strains to the same set of benzimidazole compounds. Dose responses and heritability calculations (Supplementary Fig. 5 and 6) were used to select concentrations for linkage mapping experiments. Linkage mapping was carried out with a collection of 153 recombinant inbred lines (RILs) created using the parental strains AF16 and HK104²⁴, which led to the discovery of four QTL for the tested drugs (Supplementary Fig. 7A, and Supplementary Table 6). The *C. briggsae* QTL of largest effect is found on the left arm of chromosome IV (2.56 - 3.45 Mb) and explains approximately 18% of fenbendazole-induced variation in fecundity between the parental strains (Supplementary Fig. 7B). Strikingly, this QTL falls within the primary *C. briggsae* piRNA cluster (Chr IV: 0 - 6.9 Mb). Despite tens of millions of years of evolutionary distance²⁵, the most significant *C. elegans* and *C. briggsae* benzimidazole QTL were found to occur in piRNA-enriched genomic regions that are syntenic between species²⁶. The *C. briggsae* fenbendazole QTL region contains 84 protein-coding genes with variants (Supplementary Table 7), however, none of these genes are orthologous to variant-containing genes within the *C. elegans* albendazole and fenbedazole QTL intervals. piRNA-encoding genes that densely cover this locus could potentially underlie the fenbendazole-resistance phenotype in *C. briggsae* and provide basis for a common but independent mechanism of piRNA-mediated benzimidazole resistance across species.

We report the discovery of a new mechanism of drug resistance caused by variation in regulatory piRNA genes of *C. elegans*. Our data suggest that this phenomenon may also extend to *C. briggsae*. Although the possibility of small RNA-mediated anthelmintic resistance has been speculated²⁷, this result represents the first demonstration of an experimental connection in any nematode species. Small RNA involvement in resistance to antibiotics and drugs has been reported^{28,29}, but piRNAs have not emerged as a mechanism of drug resistance. In relation to parasite disease control, the 21U-RNA/piRNA pathway is largely conserved in clade V nematodes³⁰, which include major ruminant pathogens and human hookworms. Although nematodes outside of clade V lack *prg-1*, many species express 22G RNAs and contain RNA-dependent RNA polymerases (RdRPs) responsible for 22G RNA biogenesis and transgenerational amplification. Therefore, genetic variation in these pathways should be considered as a potential basis for anthelmintic resistance in clade III and clade IV nematodes, which encompass the etiological agents of ascariasis and lymphatic filariasis, as well as plant pathogenic nematodes. The involvement of piRNAs in drug resistance presents a new source of potential molecular markers that can be deployed to monitor the development of anthelmintic resistance in the field and clinic, and raises the possibility of transgenerational inheritance of drug resistance^{31,32}. These findings put focus on a class of regulatory biomolecules that have been historically overlooked in our effort to understand and model the development of anthelmintic resistance and drug resistance at large.

Methods

High-throughput phenotyping assay

Strains were propagated for four generations to reduce or remove transgenerational effects and bleach-synchronized before transfer to 96-well growth plates (~ 1 embryo/μl in K medium). Hatched L1 larvae are fed HB101 bacterial lysate (5 mg/ml) and incubated for 48 hours at 20°C. L4 larvae are sorted into 96-well drug plates (three animals/well) using the COPAS BIOSORT large particle sorter (Union Biometrica). Drug plates contain anthelmintics dissolved in K medium at the desired final concentrations along with 1% DMSO, 10 mg/ml HB101 bacterial lysate, and 31.25 μM kanamycin. These cultures are incubated for 96 hours at 20°C to allow development to the adult stage and the maturation of deposited embryos. Animals are fed a solution of 1 mg/ml bacterial lysate and 0.01 μM red fluorescent microspheres (Polysciences, cat. 19507-5) for five minutes prior to scoring. Animals are immobilized with 50 mM sodium azide, and the COPAS BIOSORT large particle sorter is used to measure a range of animal fitness traits including length, pharyngeal pumping (red fluorescence), and brood size.

Trait generation for dose responses and linkage mapping

Raw phenotype data collected from the COPAS BIOSORT large particle sorter were processed with the R package easysorter³³. The function `read_data()` was used to distinguish animals from bubbles using a support vector machine (SVM). The functions `remove_contamination()` and `sumplate()` were used to mask contaminated wells and to calculate summary statistics across measured parameters. Parameters included time-of-flight (animal length), extinction (optical density), fluorescence (pharyngeal pumping), and total object count (brood size). Summary statistics included the mean and quantiles (10th, 25th, 50th, 75th, and 90th) for each of these parameters. Brood size was normalized to the sorted number of animals per well (n), while fluorescence was normalized to animal length (TOF). The `regress(assay=TRUE)` function was used to fit a linear model to account for differences in assays carried out on different days. Outliers were defined as observations that fall outside the IQR by at least twice the IQR and that do not group with at least 5% of the observations. Outliers were removed using the `bamf_prune()` function and `regress(assay=FALSE)` was used to fit a linear model ($\text{phenotype} \sim \text{control phenotype}$) to calculate drug effects with respect to control (DMSO solvent) conditions.

Dose responses and selection of heritable doses

The dose-dependent phenotypic effects of benzimidazoles were assayed in technical quadruplicate across four genetically diverged *C. elegans* (N2, CB4856, DL238, and JU258) and *C. briggsae* (AF16, HK104, VT847, and ED3035) strains. Phenotypes were measured using the high-throughput assay and trait generation pipeline described previously. Drug concentrations for linkage mapping experiments were selected based on broad-sense heritability calculations for traits of interest and with the goal of maximizing differences in sublethal drug effects between the parental strains used to generate recombinant lines (*C. elegans*: N2 and CB4856; *C. briggsae*: AF16 and HK104).

Linkage mapping of fitness traits

Benzimidazole exposure phenotypes were amassed for a population of 292 unique *C. elegans* recombinant inbred advanced intercross lines (RIAILs) resulting from an advanced intercross of N2 and CB4856, as well as 153 unique *C. briggsae* recombinant inbred lines (RILs) created using AF16 and HK104. These phenotypic data were gathered and processed as described above. R/qtl³⁴ was used to carry out marker regression on 1454 *C. elegans* markers and 1031 *C. briggsae* markers. QTL were detected by calculating logarithm of odds (LOD) scores for each marker and each trait as $-n(\ln(1 - r^2)/2\ln(10))$, where r is the Pearson correlation coefficient between RIAIL genotypes at the marker and phenotype trait values³⁵. Significance thresholds for QTL detection were calculated using 1000 permutations and a genome-wide error rate of 0.05. The marker with the maximal LOD score exceeding significance was retained as the peak QTL marker for each of three mapping iterations. QTL confidence intervals were defined by a 1.5 LOD drop from peak QTL markers. Broad-sense heritability was calculated using repeat measures of parental and recombinant strain phenotypes, as described previously³⁶.

Generation of near-isogenic lines

NILs were generated by backcrossing N2xCB4856 RIAILs to either parental strain for six generations, followed by six generations of selfing to homozygose the genome. Primers were optimized to genotype N2xCB4856 insertion-deletion variants immediately flanking introgression regions of interest. NIL reagents, primers, and PCR conditions are detailed in Supplemental Methods. Whole-genome sequencing at 10x depth was used to confirm the NIL genotypes.

Mutant and NIL strain phenotyping assays

C. elegans mutants (*alg-4(tm1184)*; *alg-3(tm1155)*, *ergo-1(tm1860)*, *prg-1(n4357)*), and *ben-1(tm234)* were propagated alongside N2 and CB4856 to assay albendazole-response phenotypes. The *prg-1* mutant strain was backcrossed to N2 for 10 generations. Primers and other reagents used to genotype backcross progeny are outlined in Supplementary Methods. NIL and mutant phenotyping assays were carried out with the high-throughput pipeline described above, with at least two independent biological replicates carried out for each strain panel.

RNA-Seq and Small RNA-Seq

C. elegans strains N2 and CB4856 were bleach-synchronized and grown at 20°C for isolation of total RNA from young adult animals (60 hours post-embryo plating) using a liquid N2 freeze-cracking protocol with TRIzol (Life Technologies). RNA was collected from four independent biological replicates per strain. RNA samples were treated with 20 U 5' Polyphosphatase (Epicentre) for 30 min at 37°C to convert 5'-triphosphorylated 22G-RNAs into 5'-monophosphorylated RNAs for 5' independent library construction. Sample RNA concentration and quality were assessed via Agilent Bioanalyzer. Small RNA libraries were constructed for phosphatase and non phosphatase-treated RNA samples using the TruSeq Small RNA Library Prep Kit (Illumina). mRNA libraries were prepared for non-phosphatase-treated RNA samples using the TruSeq Stranded mRNA Library Prep Kit with oligo-dT selection (Illumina). All samples were sequenced using the Illumina HiSeq 2500 platform with a single-end 50 bp read setting (University of Chicago Genomics Facility) and demultiplexed for downstream analyses.

Prediction of causal piRNAs and their target genes

Reads were adapter and quality trimmed using Trimmomatic³⁷. HiSAT2 and StringTie³⁸ were used to produce raw and TPM (transcripts per million) mRNA and 22G RNA read counts for annotated genes. DESeq2³⁹ was used to identify differentially expressed genes, as well as genes with differential 22G RNA counts. Separately, small RNA reads were used to identify variation in the piRNA complements of N2 and CB4856. Blastn⁴⁰ was used to predict targets for putative strain-unique piRNAs (21mers). mRNA and 22G expression data for the predicted gene targets of strain-specific piRNAs were used to identify putative piRNAs and gene targets causal to benzimidazole resistance. The N2 reference genome (WormBase.org⁴¹ release WS255) and associated gene annotations, the independently assembled CB4856 genome⁴², and known N2-CB4856 genome variants⁴³ were used in these pipelines, along with bwa⁴⁴, samtools⁴⁵, bedtools⁴⁶, R and Python scripts, and other command-line tools. The entire RNA and small RNA-seq pipeline (Supplementary Methods) was implemented with Nextflow⁴⁷ and is publicly available through GitHub (github.com/AndersenLab/BZRNA-seq-nf, github.com/AndersenLab/BZsmRNA-seq-nf).

Statistical analyses

Data are shown as Tukey box plots or mean ± SD as indicated in figure legends. Analyses were performed using R by two-tailed t-test (for two groups) or one-way ANOVA with Tukey's multiple comparison test (for more than two groups). P-values less than 0.05 were considered significant.

Gene interval annotation and parasite orthology analysis

C. elegans variants distinguishing N2 and CB4856⁴³ were used to annotate QTL intervals with respect to existing gene annotations. *C. briggsae* variants distinguish AF16 and HK104 as well as their estimated functional consequences were produced from genomic sequence and annotation data using SnpEff⁴⁸. For all *C. elegans* QTL not pursued in this study, parasite orthologs of genes with variants predicted to be of 'moderate' or 'high' impact were extracted with custom Python scripts. *Caenorhabditis* orthologs from the clade V ruminant parasite *Haemonchus contortus* and the clade III human filarial parasite *Brugia malayi* were extracted from WormBase⁴¹. These data are presented in Supplementary Table 8.

Data Availability

RNA sequencing data are available in the NCBI SRA under accession number [NUMBER]. Linkage mapping and phenotype data and all scripts used in the analyses of these and any other data are available through GitHub (github.com/AndersenLab/C-elegans-Benzimidazole-Resistance-Manuscript).

References

1. Hotez, P. J. *et al.* The global burden of disease study 2010: interpretation and implications for the neglected tropical diseases. *PLoS Negl. Trop. Dis.* **8**, e2865 (2014).
2. Geary, T. G. Are new anthelmintics needed to eliminate human helminthiases? *Curr. Opin. Infect. Dis.* **25**, 709–717 (2012).
3. Savioli, L. Preventive anthelmintic chemotherapy—expanding the armamentarium. *N. Engl. J. Med.* **370**, 665–666 (2014).
4. Kaplan, R. M. & Vidyashankar, A. N. An inconvenient truth: global worming and anthelmintic resistance. *Vet. Parasitol.* **186**, 70–78 (2012).
5. De Clercq, D. *et al.* Failure of mebendazole in treatment of human hookworm infections in the southern region of mali. *Am. J. Trop. Med. Hyg.* **57**, 25–30 (1997).
6. Albonico, M. *et al.* Efficacy of mebendazole and levamisole alone or in combination against intestinal nematode infections after repeated targeted mebendazole treatment in zanzibar. *Bull. World Health Organ.* **81**, 343–352 (2003).
7. Humphries, D. *et al.* Hookworm infection among school age children in kintampo north municipality, ghana: nutritional risk factors and response to albendazole treatment. *Am. J. Trop. Med. Hyg.* **89**, 540–548 (2013).
8. Adegnika, A. A., Lötsch, F., Mba, R. M. O. & Ramharter, M. Update on treatment and resistance of human trichuriasis. *Curr Trop Med Rep* **2**, 218–223 (2015).
9. Kotze, A. C. *et al.* Recent advances in candidate-gene and whole-genome approaches to the discovery of anthelmintic resistance markers and the description of drug/receptor interactions. *Int. J. Parasitol. Drugs Drug Resist.* **4**, 164–184 (2014).
10. Driscoll, M., Dean, E., Reilly, E., Bergholz, E. & Chalfie, M. Genetic and molecular analysis of a caenorhabditis elegans beta-tubulin that conveys benzimidazole sensitivity. *J. Cell Biol.* **109**, 2993–3003 (1989).
11. Lubega, G. W. & Prichard, R. K. Specific interaction of benzimidazole anthelmintics with tubulin: high-affinity binding and benzimidazole resistance in haemonchus contortus. *Mol. Biochem. Parasitol.* **38**, 221–232 (1990).

12. Kwa, M. S. G., Veenstra, J. G. & Roos, M. H. Benzimidazole resistance in *haemonchus contortus* is correlated with a conserved mutation at amino acid 200 in *nbeta*-tubulin isotype 1. *Mol. Biochem. Parasitol.* **63**, 299–303 (1994).
13. Vercruyse, J. *et al.* Assessment of the anthelmintic efficacy of albendazole in school children in seven countries where Soil-Transmitted helminths are endemic. *PLoS Negl. Trop. Dis.* **5**, e948 (2011).
14. Keiser, J. & Utzinger, J. Efficacy of current drugs against soil-transmitted helminth infections: systematic review and meta-analysis. *JAMA* **299**, 1937–1948 (2008).
15. Levecke, B. *et al.* Assessment of anthelmintic efficacy of mebendazole in school children in six countries where soil-transmitted helminths are endemic. *PLoS Negl. Trop. Dis.* **8**, e3204 (2014).
16. Jones, A. K., Buckingham, S. D. & Sattelle, D. B. Chemistry-to-gene screens in *caenorhabditis elegans*. *Nat. Rev. Drug Discov.* **4**, 321–330 (2005).
17. Ghosh, R., Andersen, E. C., Shapiro, J. A., Gerke, J. P. & Kruglyak, L. Natural variation in a chloride channel subunit confers avermectin resistance in *c. elegans*. *Science* **335**, 574–578 (2012).
18. Andersen, E. C. *et al.* A powerful new quantitative genetics platform, combining *caenorhabditis elegans* High-Throughput fitness assays with a large collection of recombinant strains. *G3* **5**, 911–920 (2015).
19. Geary, T. G. *et al.* *Haemonchus contortus*: ivermectin-induced paralysis of the pharynx. *Exp. Parasitol.* **77**, 88–96 (1993).
20. Martin, R. J. Modes of action of anthelmintic drugs. *Vet. J.* **154**, 11–34 (1997).
21. Graham Ruby, J. *et al.* Large-Scale sequencing reveals 21U-RNAs and additional MicroRNAs and endogenous siRNAs in *c. elegans*. *Cell* **127**, 1193–1207 (2006).
22. Batista, P. J. *et al.* PRG-1 and 21U-RNAs interact to form the piRNA complex required for fertility in *c. elegans*. *Mol. Cell* **31**, 67–78 (2008).
23. Sarkies, P. & Miska, E. A. Small RNAs break out: the molecular cell biology of mobile small RNAs. *Nat. Rev. Mol. Cell Biol.* **15**, 525–535 (2014).
24. Ross, J. A. *et al.* *Caenorhabditis briggsae* recombinant inbred line genotypes reveal inter-strain incompatibility and the evolution of recombination. *PLoS Genet.* **7**, e1002174 (2011).
25. Cutter, A. D., Dey, A. & Murray, R. L. Evolution of the *caenorhabditis elegans* genome. *Mol. Biol. Evol.* **26**, 1199–1234 (2009).
26. Shi, Z., Montgomery, T. A., Qi, Y. & Ruvkun, G. High-throughput sequencing reveals extraordinary fluidity of miRNA, piRNA, and siRNA pathways in nematodes. *Genome Res.* **23**, 497–508 (2013).
27. Devaney, E., Winter, A. D. & Britton, C. microRNAs: a role in drug resistance in parasitic nematodes? *Trends Parasitol.* **26**, 428–433 (2010).
28. Eyraud, A., Tattevin, P., Chabelskaya, S. & Felden, B. A small RNA controls a protein regulator involved in antibiotic resistance in *staphylococcus aureus*. *Nucleic Acids Res.* **42**, 4892–4905 (2014).
29. Zhao, L., Liu, W., Xiao, J. & Cao, B. The role of exosomes and “exosomal shuttle microRNA” in tumorigenesis and drug resistance. *Cancer Lett.* **356**, 339–346 (2015).
30. Sarkies, P. *et al.* Ancient and novel small RNA pathways compensate for the loss of piRNAs in multiple independent nematode lineages. *PLoS Biol.* **13**, e1002061 (2015).
31. Ashe, A. *et al.* piRNAs can trigger a multigenerational epigenetic memory in the germline of *c. elegans*. *Cell* **150**, 88–99 (2012).
32. Miska, E. A. & Ferguson-Smith, A. C. Transgenerational inheritance: Models and mechanisms of non-DNA sequence-based inheritance. *Science* **354**, 59–63 (2016).
33. Shimko, T. C. & Andersen, E. C. COPASutils: An R package for reading, processing, and visualizing data from COPAS Large-Particle flow cytometers. *PLoS One* **9**, e111090 (2014).
34. Broman, K. W., Wu, H., Sen, S. & Churchill, G. A. R/qtL: QTL mapping in experimental crosses. *Bioinformatics* **19**, 889–890 (2003).
35. Bloom, J. S., Ehrenreich, I. M., Loo, W. T., Lite, T.-L. V. o. & Kruglyak, L. Finding the sources of missing heritability in a yeast cross. *Nature* **494**, 234–237 (2013).
36. Brem, R. B., Storey, J. D., Whittle, J. & Kruglyak, L. Genetic interactions between polymorphisms that affect gene expression in yeast. *Nature* **436**, 701–703 (2005).

37. Bolger, A. M., Lohse, M. & Usadel, B. Trimmomatic: a flexible trimmer for illumina sequence data. *Bioinformatics* **30**, 2114–2120 (2014).
38. Pertea, M., Kim, D., Pertea, G. M., Leek, J. T. & Salzberg, S. L. Transcript-level expression analysis of rna-seq experiments with hisat, stringtie and ballgown. *Nature Protocols* **11**, 1650–1667 (2016).
39. Love, M. I., Huber, W. & Anders, S. Moderated estimation of fold change and dispersion for rna-seq data with deseq2. *Genome biology* **15**, 550 (2014).
40. Altschul, S. F., Gish, W., Miller, W., Myers, E. W. & Lipman, D. J. Basic local alignment search tool. *J. Mol. Biol.* **215**, 403–410 (1990).
41. Harris, T. W. *et al.* Wormbase: a comprehensive resource for nematode research. *Nucleic acids research* **38**, D463–D467 (2010).
42. Thompson, O. A. *et al.* Remarkably divergent regions punctuate the genome assembly of the caenorhabditis elegans hawaiian strain CB4856. *Genetics* **200**, 975–989 (2015).
43. Cook, D. E. *et al.* The genetic basis of natural variation in caenorhabditis elegans telomere length. *Genetics* **204**, 371–383 (2016).
44. Li, H. & Durbin, R. Fast and accurate short read alignment with Burrows–Wheeler transform. *Bioinformatics* **25**, 1754–1760 (2009).
45. Li, H. *et al.* The sequence Alignment/Map format and SAMtools. *Bioinformatics* **25**, 2078–2079 (2009).
46. Quinlan, A. R. & Hall, I. M. BEDTools: a flexible suite of utilities for comparing genomic features. *Bioinformatics* **26**, 841–842 (2010).
47. Kurs, J. P., Simi, M. & Campagne, F. Nextflowworkbench: Reproducible and reusable workflows for beginners and experts. *bioRxiv* 041236 (2016).
48. Cingolani, P. *et al.* A program for annotating and predicting the effects of single nucleotide polymorphisms, snpeff: Snps in the genome of drosophila melanogaster strain w1118; iso-2; iso-3. *Fly* **6**, 80–92 (2012).

Acknowledgements

The authors thank Sam Rosenberg and Robyn Tanny for help with the high-throughput phenotyping assay. The authors additionally thank Matteo Di Bernardo for help in NIL construction, as well as members of the Andersen laboratory for critical comments on the manuscript. E.C.A. is a Pew Scholar in the Biomedical Sciences, supported by the Pew Charitable Trusts. Funding for E.C.A. is also provided by a Basil O’Connor Starter Research Award from the March of Dimes Foundation and an NIH NIAID grant (R21AI121836).

Author contributions

M.Z. and E.C.A. designed the experiments, analyzed and interpreted the data, and wrote the manuscript. D.L. and J.L. provided reagents and edited the manuscript. M.Z. and D.E.C. analyzed genomic data.

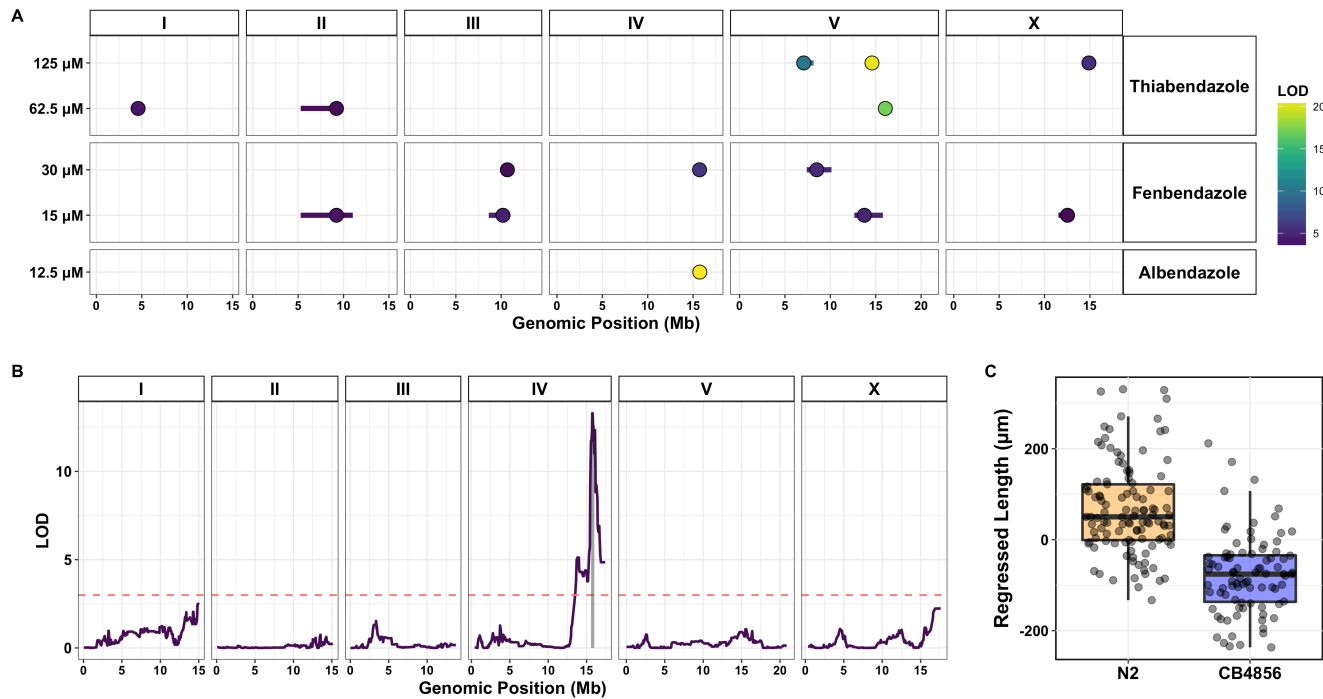


Figure 1. Discovery of benzimidazole response QTL in *C. elegans*. (A) Results of *C. elegans* linkage mapping experiments are shown for the six drug-dose conditions tested. QTL peak markers (circles) and confidence intervals (lines) are depicted. Fill color corresponds to the QTL LOD score. Overlapping QTL for a given condition are represented by the trait with the highest significance score. In total, 21 non-overlapping QTL were identified across conditions. (B) Linkage mapping plot for the QTL of highest significance depicts a major-effect QTL for albendazole sensitivity. The plot shows genomic position along the x-axis and significance (LOD score) along the y-axis. The QTL confidence interval (chromosome IV: 15.47 - 15.91 Mb) is shaded in gray and the red dashed line represents the genome-wide corrected significance threshold for the first mapping iteration (LOD score for QTL peak marker = 19.93; LOD threshold = 2.99). This QTL explains 36% of trait variation. (C) Tukey box plots showing the phenotypic split of RIAILs that have either the N2 or CB4856 genotype at the peak QTL marker position. N2 animals are significantly more resistant to albendazole exposure than CB4856 animals ($P < 0.001$).

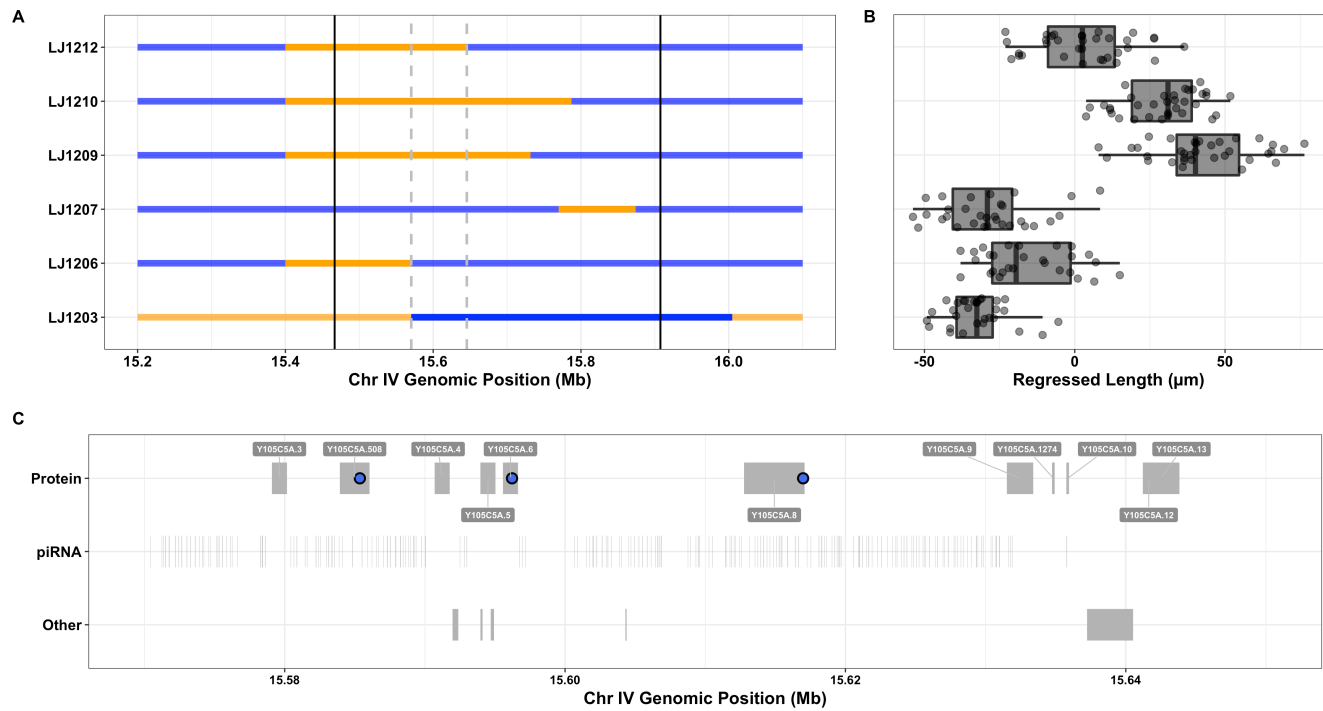


Figure 2. Narrowing of the albendazole QTL interval using near-isogenic lines. NIL genotypes (A) and corresponding Tukey box plots of NIL phenotypes (B) are shown. NIL phenotypes can be clearly classified into albendazole-sensitive (LJ1203, LJ1206, and LJ1207) and resistant groups (LJ1209, LJ1210, and LJ1212). This phenotypic separation allows for the narrowing of the QTL interval (chromosome IV: 15.47 - 15.91 Mb) to a much smaller region (chromosome IV: 15.57 - 15.65 Mb). Solid and dashed-vertical lines are used to mark the original QTL interval and the NIL-narrowed interval, respectively. (C) Variants distinguishing N2 and CB4856 within the NIL-narrowed interval are highlighted with respect to gene annotations. Candidate albendazole resistance variants include nonsynonymous and splice-donor variants in protein-coding genes (blue circles). No variants occur within genes encoding non-coding RNA biotypes (tRNAs, miRNAs, and snoRNAs).

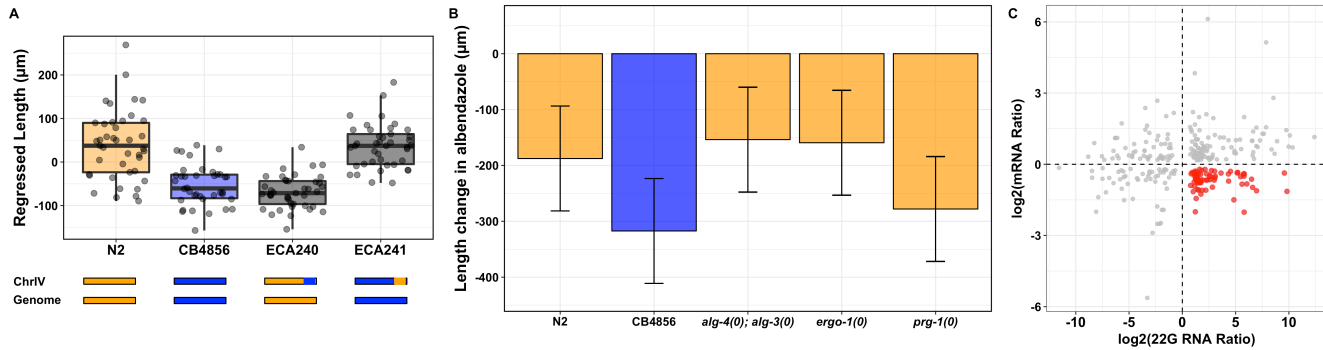
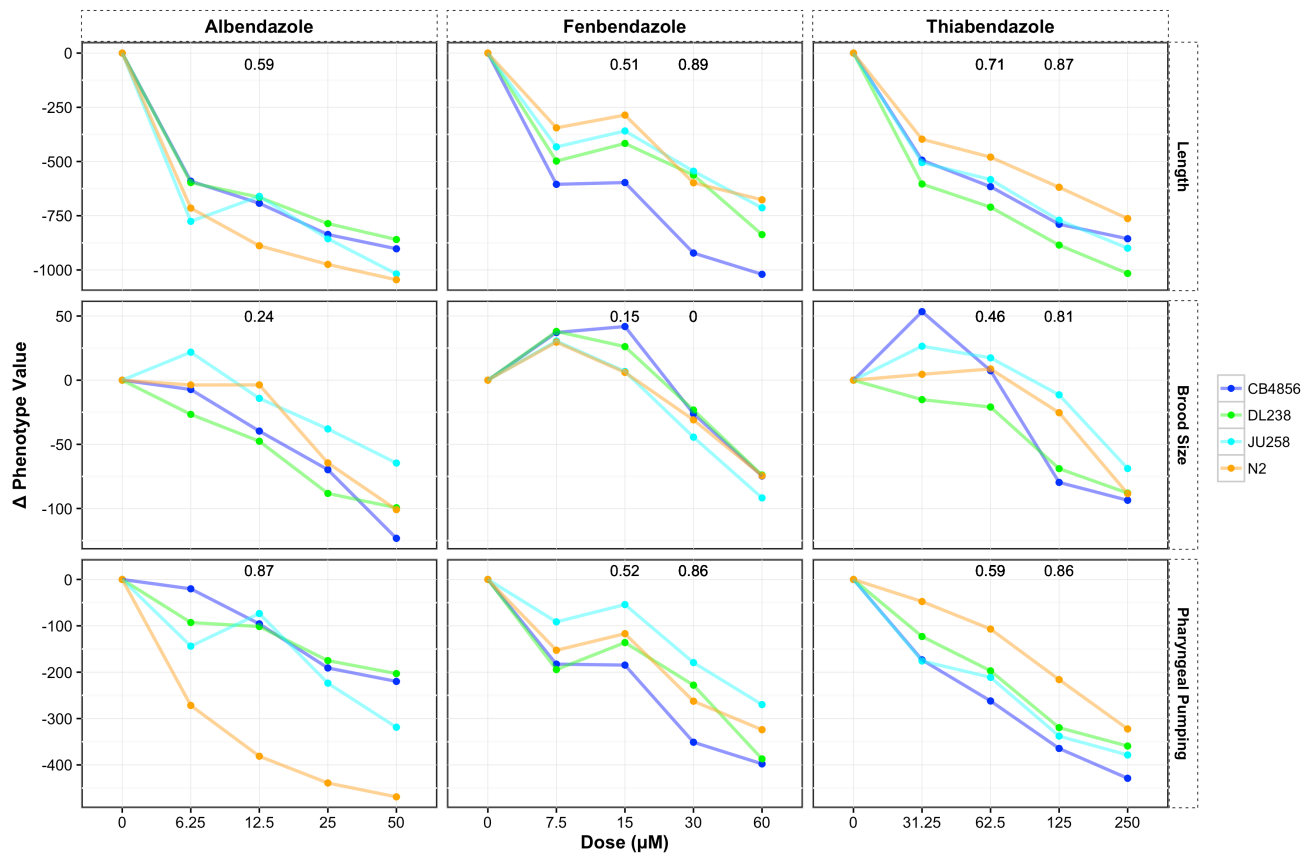


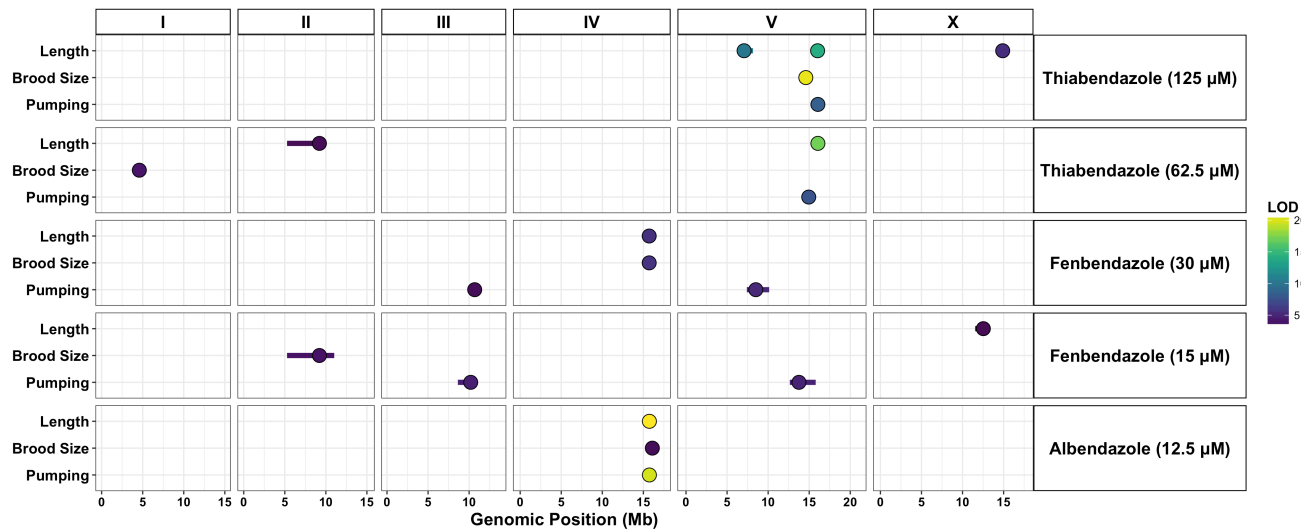
Figure 3. *C. elegans* albendazole resistance is conferred by variation in the primary piRNA cluster and is *prg-1* dependent. **(A)** Reciprocal NILs covering the primary *C. elegans* piRNA cluster (chromosome IV: 13.5 - 17.2 Mb) were phenotyped in the presence of 12.5 μM albendazole. Introgression of the piRNA cluster from CB3856 into N2 (ECA240) produces an albendazole sensitivity phenotype equivalent to the parental CB4856 strain ($P < 0.001$). Introgression of the piRNA cluster from N2 into CB4856 (ECA241) confers an albendazole resistance phenotype equivalent to N2 ($P < 0.001$). **(B)** Argonaute mutants that converge on the WAGO 22G RNA pathway were phenotyped in 12.5 μM albendazole (data are mean \pm SD). *ergo-1* and *alg-3*; *alg-4* mutants, which interact with distinct classes of 26G RNAs, do not alter the albendazole-resistance phenotype in the N2 genetic background. Loss of *prg-1*, the primary Argonaute associated with 21U-RNA/piRNA activity, confers albendazole sensitivity in the N2 background (*prg-1(0)*(orange) vs N2: $p < 0.001$). **(C)** Scatter plot of mRNA and 22G RNA expression data for gene prioritization. Axes show \log_2 fold-change of anti-sense 22G RNA and mRNA expression levels for 238 genes that are expressed in both strains (TPM > 1 across all replicates) and that show differential expression of both mRNA and 22G RNA expression ($P < 0.05$). Red points depict 68 genes that exhibit lower N2 mRNA expression coupled to higher N2 22G RNA expression.

Supplementary Information

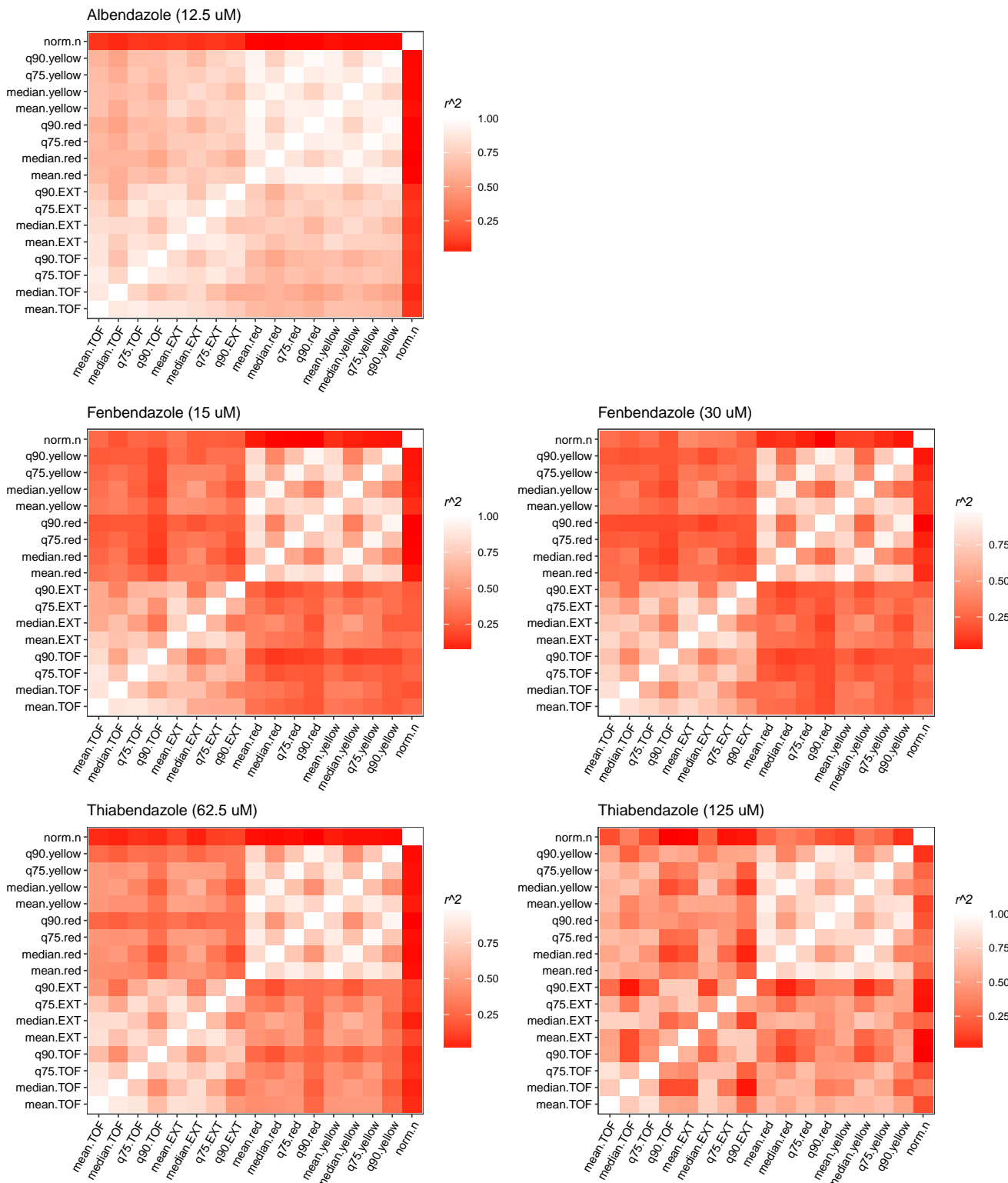
Supplementary Figure 1. *C. elegans* benzimidazole dose responses and heritability calculations. Dose responses were carried out with four genetically-diverged strains of *C. elegans*. Phenotypic responses to three drugs are shown with a representative trait for each primary trait group (length, brood size, and pharyngeal pumping). Heritability values are shown for doses used in subsequent linkage mapping experiments.



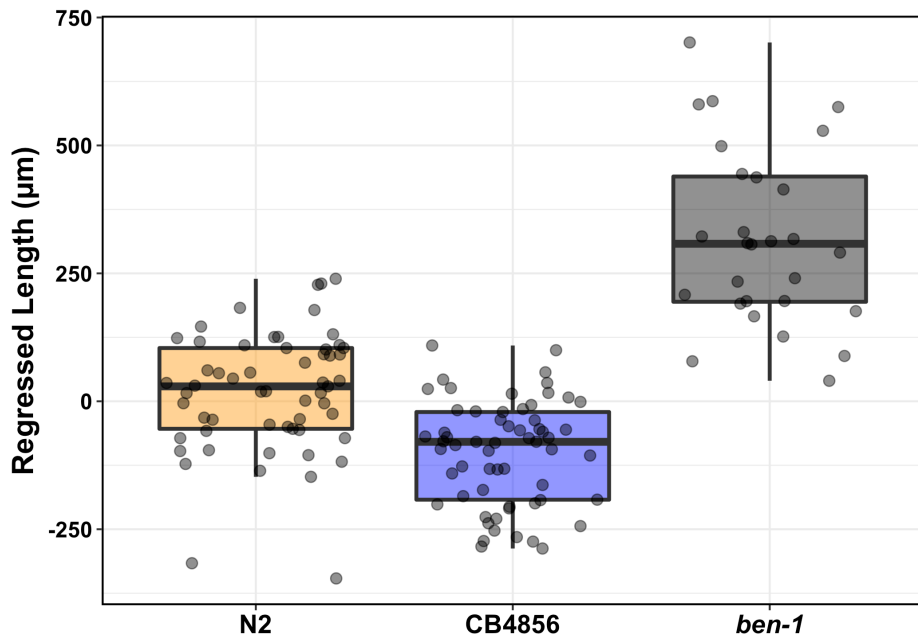
Supplementary Figure 2. *C. elegans* benzimidazole QTL grouped by drug and trait. Results of *C. elegans* linkage mapping experiments are shown for the five drug-dose conditions tested and separated by correlated trait group. QTL peak markers (circles) and confidence intervals (lines) are depicted. Fill color corresponds to the QTL LOD score. Overlapping QTL for a given condition-trait group pair are represented by the trait with the highest significance score.



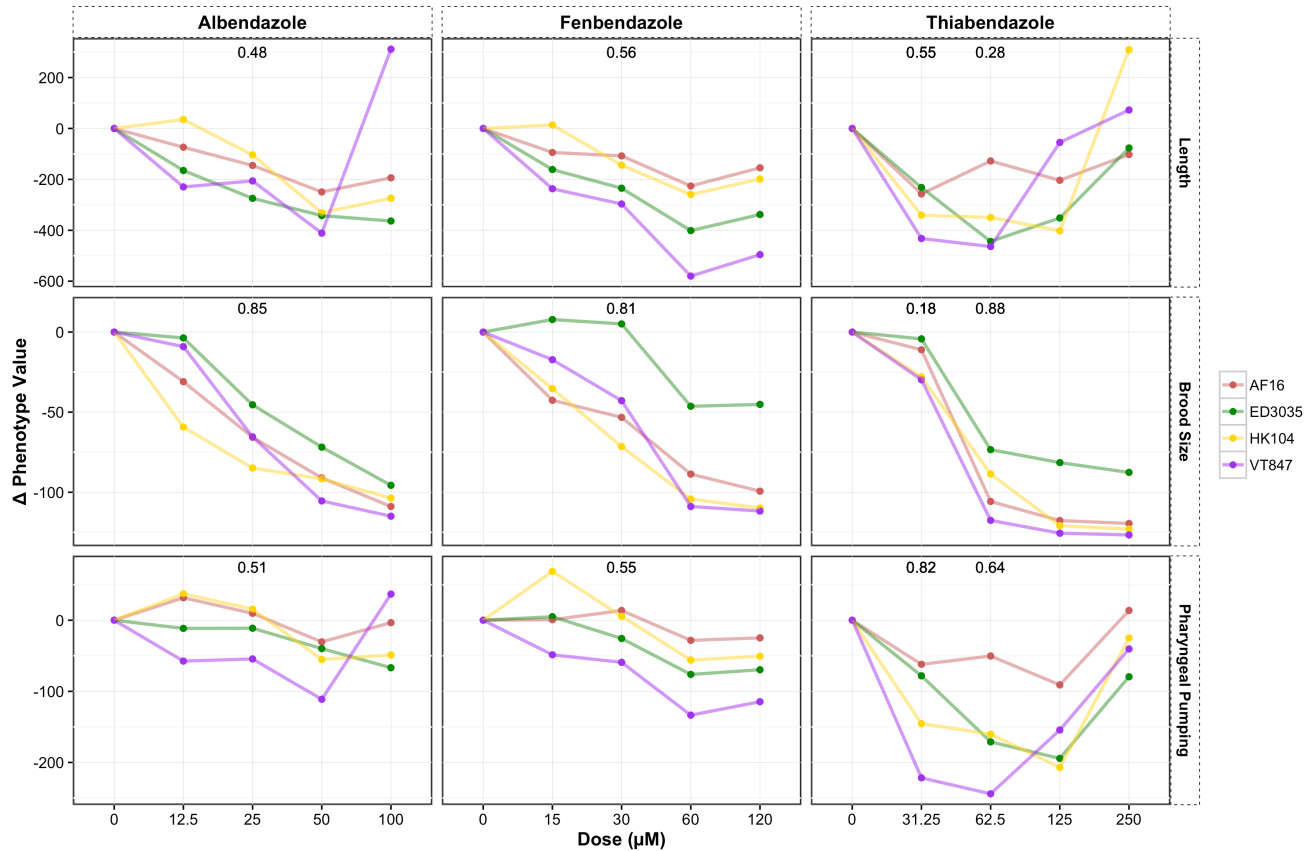
Supplementary Figure 3. *C. elegans* summary statistic correlations for primary trait groupings. The correlation structure (Pearson's correlation coefficient) of summary statistics for measured parameters of animal size (time-of-flight (TOF) and optical density (EXT)), pharyngeal pumping (red and yellow fluorescence), and brood size (norm.n) are shown for each drug and dose combination used in linkage mapping.



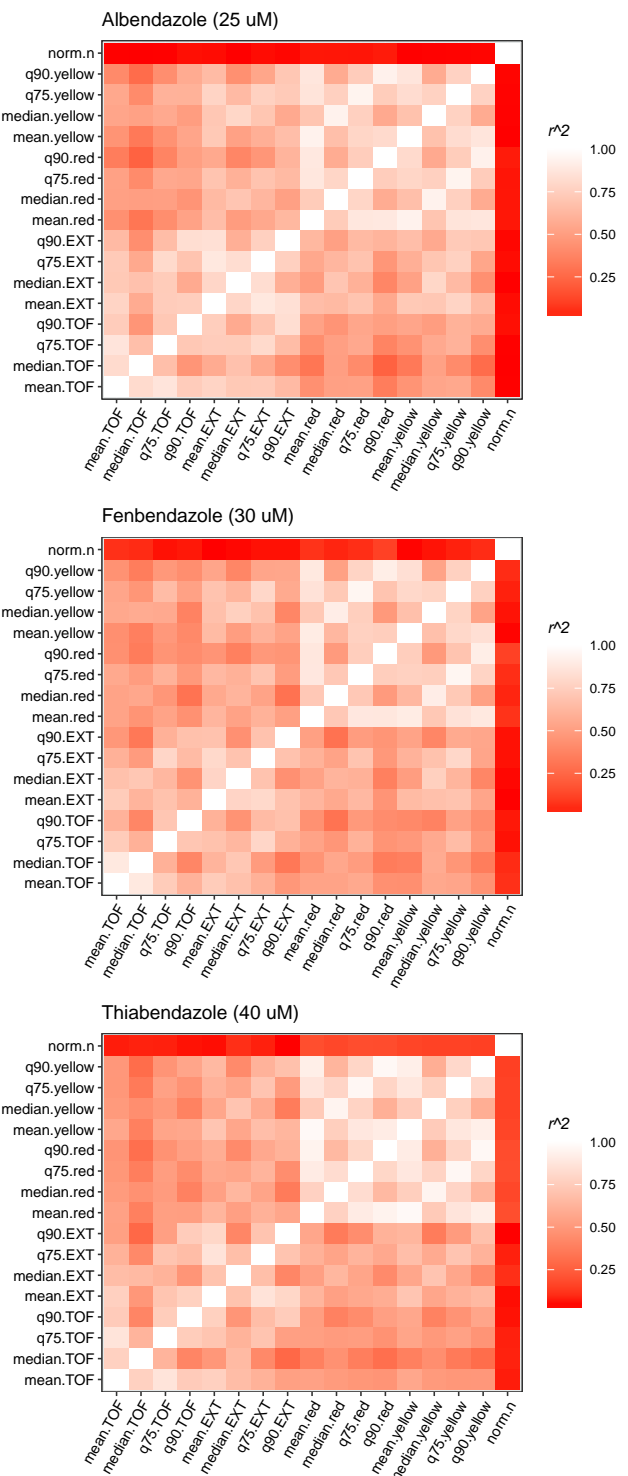
Supplementary Figure 4. Differences in *C. elegans* albendazole response between the N2 and CB4856 strains are significant with respect to resistance mediated by *ben-1* loss-of-function. Tukey box plot showing the effect of 12.5 μ M albendazole on worm length (75th quantile shown) for N2, CB4856, and a *ben-1* mutant in the N2 genetic background (all pair-wise differences are statistically significant; $P < 0.001$). The differences in the means of the two parental strains are approximately 45% of the difference between the means of N2 and the *ben-1* mutant.



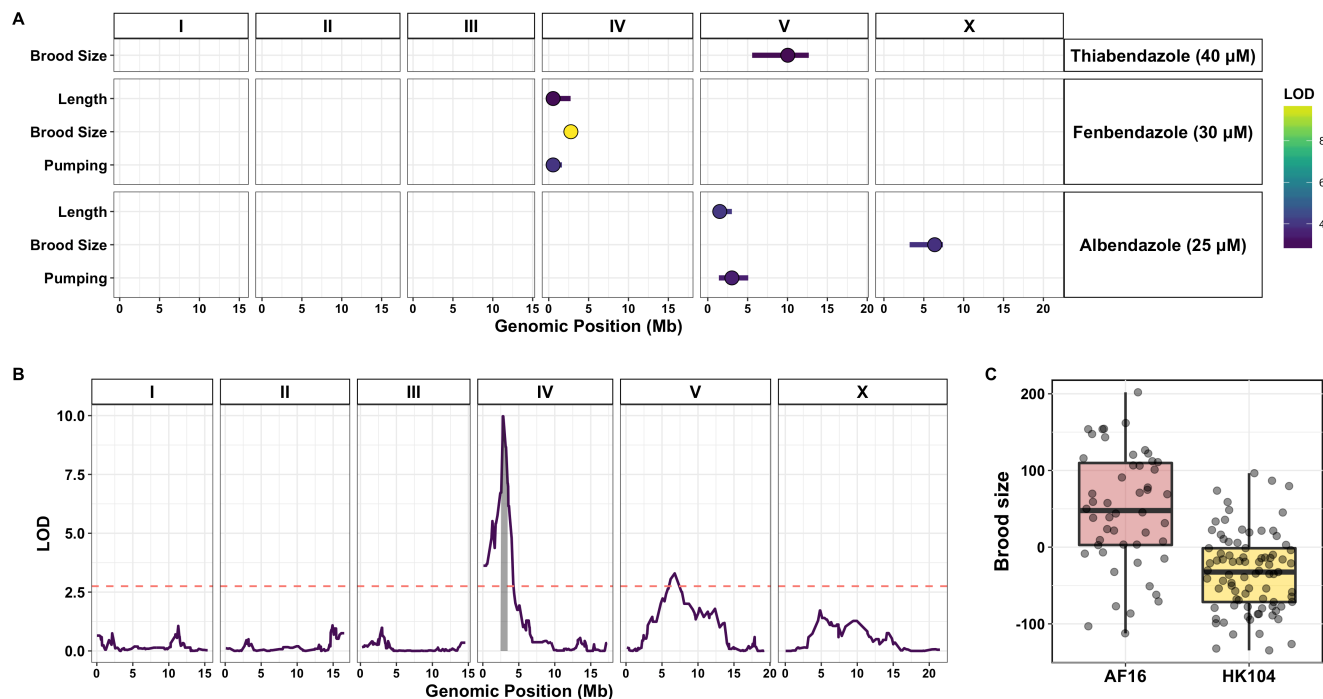
Supplementary Figure 5. *C. briggsae* benzimidazole dose responses and heritability calculations. Dose responses were carried out with four genetically diverged strains of *C. briggsae*. Phenotypic responses to three drugs are shown with a representative trait for each primary trait group (length, brood size, and pharyngeal pumping). Heritability values are shown for doses used in subsequent linkage mapping experiments. For thiabendazole, we selected a linkage mapping dose ($40 \mu\text{M}$) that falls between the concentrations where heritability is shown.



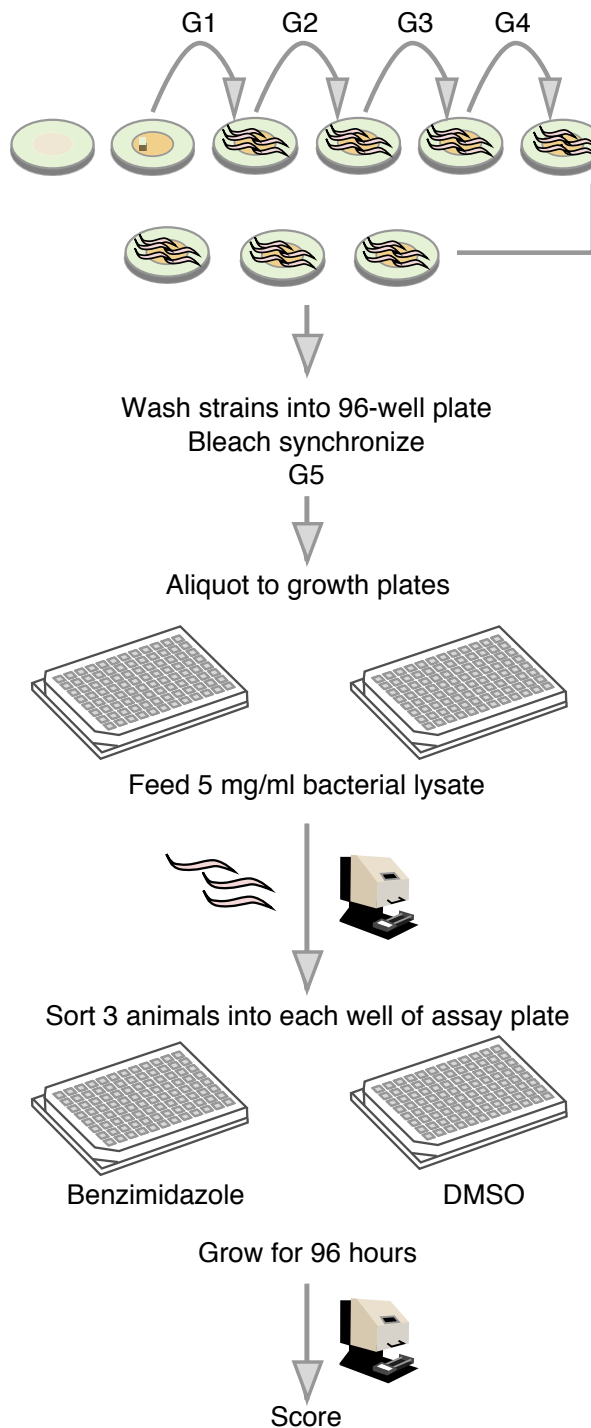
Supplementary Figure 6. *C. briggsae* summary statistic correlations for primary trait groupings. The correlation structure (Pearson's correlation coefficient) of summary statistics for measured parameters of animal size (time-of-flight (TOF) and optical density (EXT)), pharyngeal pumping (red and yellow fluorescence), and brood size (norm.n) are shown for each drug tested.



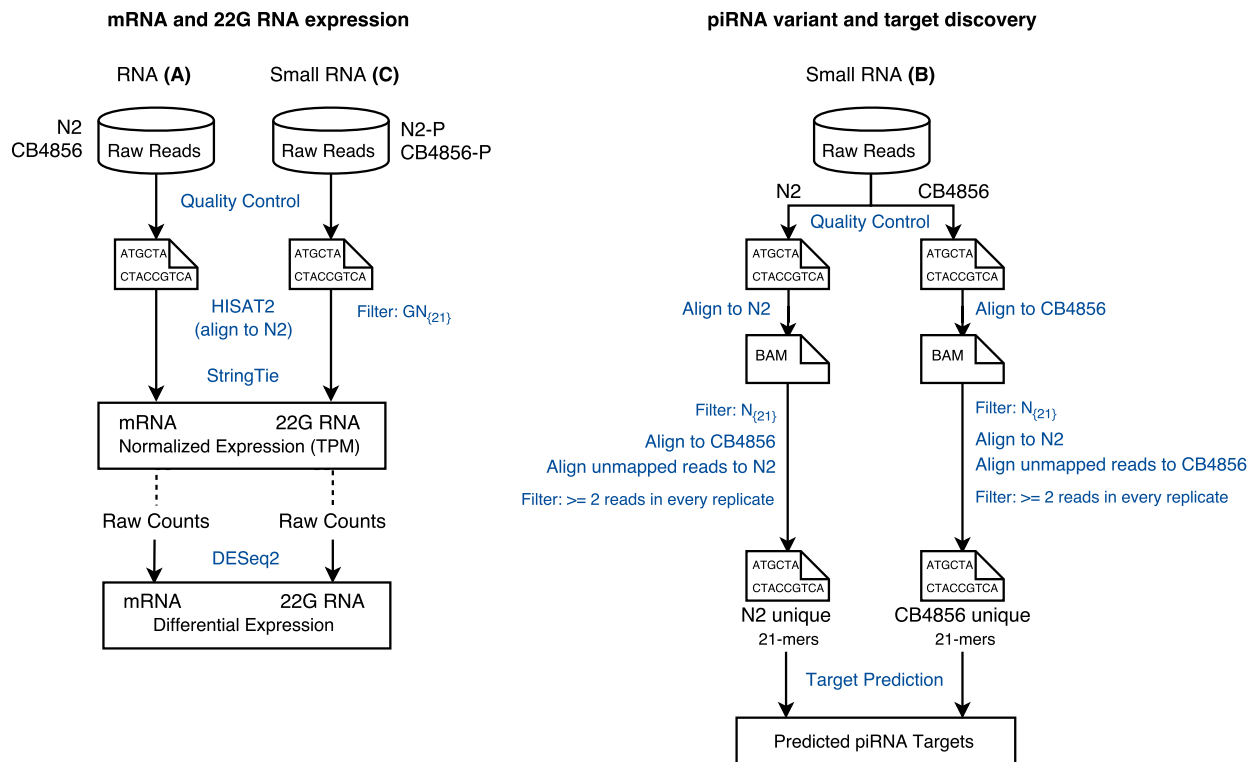
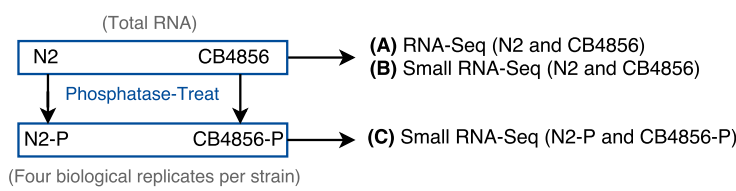
Supplementary Figure 7. Discovery of benzimidazole response QTL in *C. briggsae*. (A) Results of *C. briggsae* linkage mapping experiments are shown for three tested drugs as grouped by trait category. QTL peak markers (circles) and confidence intervals (lines) are depicted. Fill color corresponds to the QTL LOD score. In total, four non-overlapping QTL were identified across conditions. (B) Linkage mapping plot for the QTL of highest significance depicts a major-effect QTL associated with the effect of fenbendazole on brood size. The plot shows genomic position along the x-axis and significance (LOD score) along the y-axis. The QTL confidence interval (chromosome IV: 2.56 - 3.45 Mb) is shaded in gray and the red dashed line represents the genome-wide correction significance threshold for the first mapping iteration (LOD score for QTL peak marker = 9.97; LOD threshold = 2.75). This QTL explains 18% of trait variation (effect size = 0.70). (C) Tukey box plots showing the phenotypic split of RILs that have either the AF16 or HK104 genotype at the peak QTL marker position. AF16 animals are significant more resistant to fenbendazole exposure than HK104 animals ($P < 0.001$), exhibiting much larger brood sizes in the presence of drug.



Supplementary Methods 1. High-throughput sorter assay. Assay details described in main Methods section.



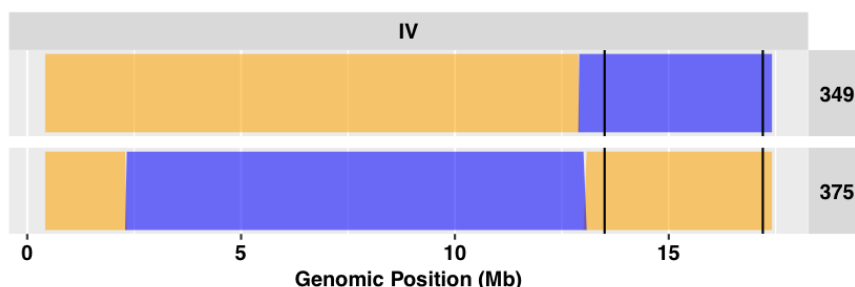
Supplementary Methods 2. piRNA variant discovery and target gene prediction pipeline. (**Top**) N2 and CB4856 RNA and small RNA was collected across drug-exposed life cycle time points and pooled into mixed-stage RNA samples for sequencing as described in Methods. (**Left**) RNA (N2 and CB4856) and small RNA (N2-P and CB4856-P) reads were aligned to the N2 genome with bwa. Small RNA reads were filtered for 22-mers beginning with a G (22G reads). Bedtools was used to count reads mapping to gene features extracted from the WS255 release canonical gene set. Only 22G reads in the opposite anti-sense to gene features were retained. RNA and 22G-RNA counts were processed further in R. (**Right**) Non phosphatase-treated RNA reads from N2 and CB4856 were aligned to their respective genomes using bwa (0 mismatches). Reads were filtered with a length requirement of 21 and only reads that fell within the broad primary piRNA cluster were kept (ChrIV: 13.5 - 17.2 Mb). N2 surviving reads were aligned to the CB4856 genome, and conversely, CB4856 surviving reads were aligned to the N2 genome. Unmapped reads with read support ≥ 2 were retained as the pool of reads unique to each strain. 21-mers unique to N2 and CB4856 were considered putative piRNAs and their gene targets were predicted using Blast (blastn-short with 80% query coverage). RNA and 22-G RNA expression data was extracted for all predicted targets of piRNAs unique to either strain and used to prioritize candidate piRNAs and target genes causal to resistance.



Supplementary Methods 3. Reagents related to NIL and mutant strain assays. **(Top)** Primers and starting RIAILs used in the construction of whole piRNA-interval NILs. **(Bottom)** Mutant strain IDs, primers, and PCR conditions used to confirm and propagate mutant alleles through back-crossing.

C. elegans whole piRNA interval NILs

- piRNA interval: Chr IV: 13.5 - 17.2 Mbs
- Left Primers (InDel Left: 13207120)
 - oECA904: aacagataactcgccgttgct
 - oECA905: atttgtaccacgctggacct
 - N2 Size: 526, CB4856 Size: 942
- Right Primers (InDel Right: 17356993)
 - oECA910: gacaacgcccactacgacaaa
 - oECA911: acccaaccaggatggacacat
 - N2 Size: 443, CB4856 Size: 596
- CB4856>N2 NIL
 - **ECA240** / eanIR160 (IV, CB4856>N2)
 - Starting RIAIL: QX349
- N2>CB4856 NIL
 - **ECA241** / eanIR161 (IV, N2>CB4856)
 - Starting RIAIL: QX375



C. elegans mutants

- piRNA mutants confirmed and/or backcrossed in N2 background
 - ECA270: alg-4(tm1184);alg-3(tm1155) [ALG-3/4 class 26G RNA]
 - ECA271: WM158 / ergo-1(tm1860) [ERGO-1 class 26G RNA]
 - ECA286: prg-1(n4357) [21-U RNA]: SX922/ECA269 backcrossed to N2 (9x) and selfed (6x)
 - FX234: ben-1
- Mutant confirmation PCR primers
 - ergo-1(tm1860): oECA1033 AAGCGTACGAACCCGAGCTT / oECA1034 GAGCGGCTGCTCAGAAGACT
- prg-1(n4357) PCR primers for backcrossing
 - oECA1019: AGTCGTGGTACAGATCGTAG
 - oECA1020: GAGAGGCCGTGGTCAGGAT
 - Wild-type size = 1972, prg-1(n4357) size = 1248 (724 bp deletion)
 - PCR parameters: Annealing T = 55.5C, Extension time = 2:30

Supplementary Data

Supplementary Table 1. *C. elegans* QTL that explain > 5% of trait variation for all drug-dose combinations tested. Each QTL that was discovered for defined trait groups is annotated with its peak position, confidence interval, estimated variance explained, and effect size.

Supplementary Table 2. *C. elegans* protein-coding gene variants within the albendazole QTL interval. Previously defined variants distinguishing N2 and CB4856 were annotated based on predicted effects on protein function or expression. Variants of "moderate" or "high" effect are shown for the QTL and the NIL-narrowed interval.

Supplementary Table 3. *C. elegans* piRNA genes within the albendazole QTL interval. The genomic coordinates, gene IDs, and feature IDs of annotated piRNA genes within the QTL and NIL-narrowed intervals are provided.

Supplementary Table 4. Putative strain-specific piRNAs detected through sequencing. Sequences are shown for 21mers that map to the QTL region of the N2 genome but not the CB4856 genome ("N2-unique" in "strain-specificity" column), as well as 21mers that map to the corresponding QTL region of the CB4856 genome but not the N2 genome ("CB4856-unique" in "strain-specificity" column). N2-unique piRNA coordinates are provided based on the N2 genome, and CB4856-unique piRNA coordinates are provided based on the separately assembled CB4856 genome.

Supplementary Table 5. Results of RNA and small RNA-seq expression and piRNA variant and target prediction pipeline. Fold-change differences in mRNA and 22G RNA expression and associated adjusted p-values from DESeq2 analysis is shown (columns "Rlog2FC" through "Gpadj"). Normalized mRNA and 22G RNA expression values (TPM) are shown for individual biological replicates (columns "N2_A_R TPM" through "CB_D_G TPM"). Gene annotations are provided, as well as other parameters used to prioritize targets (column "Anticorr": anti-correlation of mRNA and 22G expression; column "Direction": direction of effect on mRNA expression). Predicted target sites of strain-unique piRNAs in cases of gene overlap (columns "Query" through "Tend").

Supplementary Table 6. *C. briggsae* QTL that explain > 5% of trait variation for all drugs tested. Each QTL that was discovered for defined trait groups is annotated with its peak position, confidence interval, estimated variance explained, and effect size.

Supplementary Table 7. *C. briggsae* protein-coding gene variants within the fenbendazole QTL interval. Variants distinguishing AF16 and HK104 were annotated based on predicted effects on protein function or expression. Variants of "moderate" or "high" effect are shown for the QTL and the NIL-narrowed interval.

Supplementary Table 8. Parasite (*H. contortus* and *B. malayi*) orthologs for all *C. elegans* QTL identified.